Quantum Dynamical Rate Constant for the H + O_3 Reaction Using a Six-Dimensional Double Many-Body Expansion Potential Energy Surface

H. Szichman,[†,‡] M. Baer,[§] and A. J. C. Varandas*[,†]

Departamento de Química, Universidade de Coimbra, 3049 Coimbra Codex, Portugal, and Department of Physics and Applied Mathematics, Soreq NRC, Yavne 81800, Israel

Received: May 30, 1997[⊗]

We present a quantum mechanical, three-dimensional, infinite-orden-sudden-approximation study of the H + O_3 atmospheric reaction using a recently reported double many-body expansion potential energy surface for ground-state HO_3. The results are compared with existing experimental data and previously reported quasiclassical trajectory calculations which employed the same interaction potential. Agreement with the recommended experimental data is moderate, but encouraging when compared with the data of Clyne and Monkhouse, which extends over the range of temperatures $300 \leq T/\mathrm{K} \leq 650$, and with the recent measurement of Greenblatt and Wiesenfeld for $T = 300$ K. In comparison with the classical trajectory results, the agreement is also moderate, the differences being attributed to both methodological approximations in the quantum formalism and the problem of zero-point energy leakage in classical dynamics.

1. Introduction

The H + O_3 chain-branching reaction has been much studied experimentally[1−13] due to its key role in atmospheric chemistry. It is responsible for nascent hydroxyl radicals in vibrationally excited states and for the hydroxyl spectra[14−17] in night-sky airglow. Thus, it is not surprising that there have been many experimental measurements of the H + $O_3 \rightarrow$ HO + O_2 thermal rate coefficient. Several experimental studies of the energy partitioning in the products have also been reported for the title reaction.[1,3,18,19] They suggest that the majority of the available energy (the exothermicity of the reaction H + $O_3 \rightarrow$ HO + O_2 is *ca.* 81 kJ mol^{-1}) is released as vibrational excitation of the HO product, with the upper vibrational levels ($v = 7-9$) being the most populated ones.

Theoretically, only one study of the H + O_3 reaction has been reported which used a fully six-dimensional interaction potential. In this study, Varandas and Yu[20,21] have employed the quasiclassical trajectory (QCT) technique to carry out the dynamics, while for the potential energy surface they have adopted their own analytical form[20] based on the double many-body expansion[22] (DMBE) method. This single-valued function for ground-state HO_3 has been modeled at short distances from a fit to newly reported[20] accurate ab initio energies based on unrestricted configuration-interaction calculations including singles and doubles excitations (UCISD), while a realistic description of the long-range forces has been warranted by accommodating other theoretical/empirical information in the calibration procedure. The agreement between the QCT results and the experimental rate constant measurements was considered to be fairly good[20,21] (see also section 5), although less satisfactory[21] in what refers to the energy distribution in the products. Despite these encouraging results, a counterverification of the accuracy of the HO_3 DMBE potential energy surface and the subsequent QCT dynamics study by using an alternative method of investigation, such as one based on quantum dynamics, was judged to be valuable. This is especially true since a light hydrogen atom is involved, and hence quantum effects are likely to play a significant role; this point is discussed further in the next paragraph.

For this purpose, we present an approximate quantum dynamical study of the rate constant for the title reaction using a slightly modified version (see ref 23) of a method reported previously[24−26] in a study of the reactions O + $O_3 \rightarrow 2O_2$ and H + $H_2O \rightarrow H_2$ + OH (for a related method of the infinite-orden-sudden-approximation (IOSA) type, see ref 27). Thus we implicitly consider two well-known difficulties of the classical dynamics approach (for a review, see ref 28). One refers to the inclusion of tunneling of the light hydrogen atom; the other refers to the shortcoming of classical dynamics which is due to leakage of the quantum zero-point vibrational energy. While tunneling is a purely quantum effect that enhances reactivity near threshold in comparison to a classical treatment, zero-point energy leakage is known to have an opposite effect by converting the quantum zero-point vibrational energy into translational energy which then becomes available classically to promote reaction. In fact, this is a well-known problem of classical dynamics that has attracted considerable attention in recent years,[29−46] being responsible in classical bimolecular dynamics for the formation of products with less than zero-point value. Thus, the above shortcomings of classical dynamics make it extremely difficult to obtain an accurate estimate of reactivity near threshold.

The paper is organized as follows. In section 3, we provide a brief review of the theory, while the numerical details are given in section 4. Section 5 presents the results and the discussion. The conclusions are in section 6.

2. Potential Energy Surface

The potential energy surface of HO_3 has been described in detail elsewhere,[20] and hence we focus here on its major topographical features. These are shown in Figure 1, which presents a perspective view for a H atom moving coplanarly around an equilibrium O_3 molecule. Note that the middle oxygen atom of ozone is fixed at the origin and that the three distinct stationary points (which appear as minima for a relaxed planar HO_3) correspond to the cis HO_3, trans HO_3, and C_{2v} HO_3 transition states. Clearly, there are significant orientational

[‡] On leave from Department of Physics and Applied Mathematics, Soreq NRC, Yavne 81800, Israel.
[†] Universidade de Coimbra.
[§] Soreq NRC.
[⊗] Abstract published in *Advance ACS Abstracts,* November 1, 1997.

S1089-5639(97)01760-X CCC: $14.00

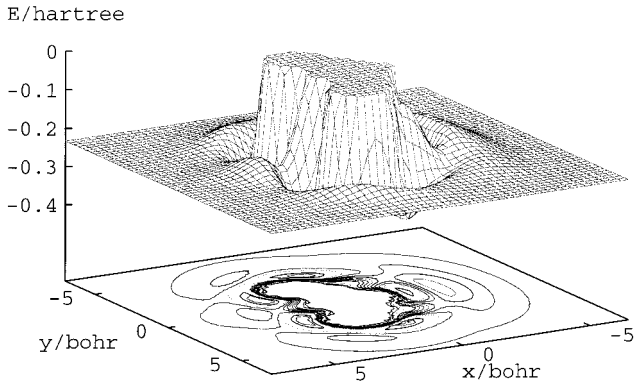

Figure 1. Perspective view for a hydrogen atom moving coplanarly around an equilibrium ozone molecule, the central atom of which is at the origin. The high plateaus may be used as reference to locate the positions of the three oxygen atoms. In the base plot, the lowest contour (in gray) corresponds to $-0.314E_h$ and the spacing between contours is $0.021E_h$.

effects in the H−O_3 interaction; in particular we observe that a very high barrier must be overcome for the H + O_3 reaction to take place when the hydrogen atom attacks the central oxygen atom of ozone. Such a barrier is considerably reduced for angles of attack close to that corresponding to H−O bond breaking in HO_3 (at equilibrium, this species has C_1 geometry). We further note that the barrier for H attacking a terminal O atom is lowest for an out of plane approach, and hence the HO_3 DMBE potential energy surface used in the present work predicts a nonlinear HOO structure at the saddle point for reaction; the reader is referred to ref 20 for further details. It should also be pointed out that there is no barrier along the minimum energy reaction path (except for a small one lying above the H···O_3 van der Waals species but below H + O_3), although as it will be shown in section 5, this by no means implies that there is no activation energy in the kinetics of the title reaction.

3. Quantum Dynamics Approach

As described elsewhere,[23−26] our method is based on the calculation of all nonreactive probabilities, i.e., $P(t \leftarrow t_0)$, and subtracting their sum from unity to obtain in this way the total reactive probability. Thus, we may write

$$P_{\text{react}} = 1 - \sum_t |S(t \leftarrow t_0)|^2 \tag{1}$$

where $S(t \leftarrow t_0)$ is an inelastic state-to-state **S** matrix element, and t (and t_0) stands for a set of quantum numbers that label a state of the four-atom system.

The matrix element $S(t \leftarrow t_0)$ can be written as

$$S(t \leftarrow t_0) = [\delta_{tt_0} + \mathrm{i}Q(t,t_0)] \exp(\mathrm{i}\phi_t) \tag{2}$$

where δ_{tt_0} is the Kronecker delta function, ϕ_t is the (elastic) tth phase shift, and $Q(t,t_0)$ is given in the form

$$Q(t,t_0) = \langle \psi_t | V | (\chi_{t_0} + \psi_{t_0}) \rangle \tag{3}$$

In eq 3, ψ_t represents the tth quantum mechanical (QM) solution of an unperturbed (elastic) Schrödinger equation, namely

$$(E - H_0)\psi_t = 0 \tag{4}$$

In turn, χ_{t_0} can be obtained by solving the following inhomogenuous Schrödinger equation in the close-interaction region:

$$(E - H_I)\chi_{t_0} = V\psi_{t_0} \tag{5}$$

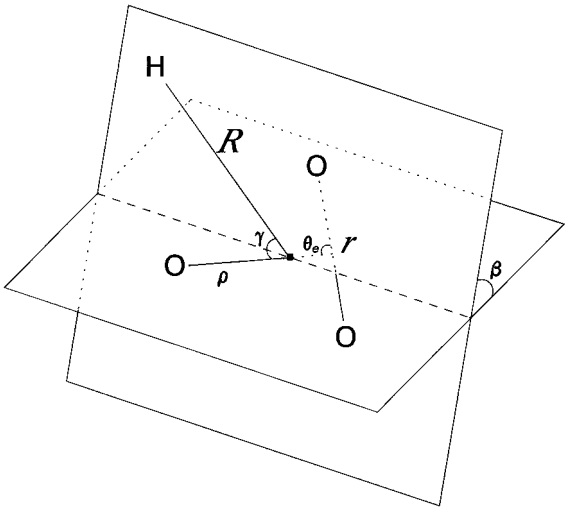

Figure 2. Coordinates used for the quantum dynamics calculations on the title reaction. For simplicity, the diagram assumes a coplanar attack.

where V is an interaction (perturbation) potential defined by

$$V = H - H_0 \tag{6}$$

Thus, H is the full Hamiltonian and H_I is ad hoc obtained, by adding to H negative imaginary potentials (NIPs) defined along the boundaries of the arrangement channel in which ψ_t is calculated. The function of these NIPs is to decouple one arrangement channel from all others and provide bound-state-like boundary conditions.[47]

Finally, development of eq 2 allows us to find two types of expressions for the nonreactive state-to-state scattering probabilities, according to whether the transition is elastic (i.e., the initial and final internal quantum numbers are identical) or inelastic:

$$P(t \leftarrow t_0) = \begin{cases} |1 - \mathrm{i}\langle \psi_t | V | (\chi_{t_0} + \psi_{t_0}) \rangle|^2; & t = t_0 \\ |\langle \psi_t | V | (\chi_{t_0} + \psi_{t_0}) \rangle|^2; & t \neq t_0 \end{cases} \tag{7}$$

3.1. Derivation of the Unperturbed Wave Functions in the Asymptotic Region. A Jacobi coordinate system is used here to describe both arrangement channels of the four-atom system (see Figure 2). Thus, the atom−triatom (reagent) channel is described by three radial distances and three Jacobi angles. The former consist of the vibrational coordinate for the unbroken bond r, the corresponding "translational" coordinate of the triatom ρ connecting the third atom with the center of mass of the unbroken bond, and the translational coordinate R which connects the fourth atom to the center of mass of the triatomic system. Three Jacobi angles then complete the description of the system: θ (the angle between r and ρ); γ (the angle between ρ and R); and β (polar angle between the triatom plane and R). The difference from ref 48 is that β is treated here as a quantum mechanical continuous variable. In fact, the main feature in this new treatment is that the following 5D *polar angle* averaged potential energy surface is used for the reactant arrangement channel,

$$\bar{U}(r\rho R\theta\gamma) = \frac{1}{\pi}\int_0^\pi U(r\rho R\theta\gamma\beta)\, \mathrm{d}\beta \tag{8}$$

while β has been fixed in the previous studies.[23−26]

To calculate ψ_t (and similarly for χ_{t0}), the following Hamiltonian should be considered.[48]

$$H_0 = -\frac{\hbar^2}{2mr}\frac{\partial^2}{\partial r^2}r - \frac{\hbar^2}{2\mu\rho}\frac{\partial^2}{\partial \rho^2}\rho - \frac{\hbar^2}{2MR}\frac{\partial^2}{\partial R^2}R + \frac{\vec{j}^{\,2}}{2mr^2} + \frac{(\vec{K}-\vec{j})^2}{2\mu\rho^2} + \frac{(\vec{J}-\vec{K})^2}{2MR^2} + \bar{U}_0(r\rho R\theta\gamma) \quad (9)$$

where the averaged potential energy surface has been used, and m, μ, and M are respectively the reduced masses of the unbroken bond, the triatomic molecule, and the whole atom+triatom system. On the other hand, $\vec{j}$ and $\vec{K}$ represent the bend and rotational angular momenta of the triatomic molecule, and $\vec{J}$ is the total angular momentum.

In general we distinguish between the asymptotic region and the short interaction region. The Schrödinger equation that follows by employing the Hamiltonian defined in eq 9 is treated twice: once to calculate the asymptotic (unperturbed) elastic wave function ψ_t and once to calculate χ_{t0}. In this paragraph we start by considering the expression of the (unperturbed) potential energy surface to be used for the solution of ψ_t (see eq 4), and which is given by

$$\bar{U}_0(r\rho R\theta\gamma) = v(r\rho\theta) + w(R) \quad (10)$$

where the potential of the O_3 molecule $v(r\rho\theta)$ follows from

$$v(r\rho\theta) = \lim_{R\to\infty} U(r\rho R\theta\gamma\beta) \quad (11)$$

and the distortion potential $w(R)$ is defined as

$$w(R) = \bar{U}(R\rho_e r_e \theta_e \gamma) \quad (12)$$

Note that ρ_e, r_e, and θ_e are obtained from the equilibrium properties of the ozone system,[49] while γ is the IOSA angle,[24−26] which is treated as a parameter, not as a variable.

In solving eq 4 the j_z approximation[50,51] has been also applied; namely the operators $(\vec{K}-\vec{j})^2$ and $(\vec{J}-\vec{K})^2$ have been replaced by

$$(\vec{K}-\vec{j})^2 \equiv \hbar^2[K(K+1) - 2\Omega_K^{\,2}] + \vec{j}^{\,2} \quad (13)$$

$$(\vec{J}-\vec{K})^2 \equiv \hbar^2[J(J+1) + K(K+1) - 2\Omega^2] \quad (14)$$

where Ω_K and Ω may take the following allowed values:

$$|\Omega_K| \le Min(K,j) \quad (15)$$

$$|\Omega| \le Min(K,J) \quad (16)$$

For more details, the reader is referred to ref 48.

3.2. The Derivation of the Perturbed Function χ_{t0}. The function χ_{t0} is derived by solving eq 5 in the reagent arrangement channel. For that purpose the range of the reagents vibrational coordinate(s) are enlarged so as to comprise the relevant reactive regions and include the necessary decoupling NIPs. In our particular case, namely the HO_3 system, the ozone molecule is characterized to have a triangular structure with one nonequivalent O atom serving as vertex, while the two remaining terminal oxygen atoms may interchange positions between them. The attacking hydrogen may then react alternatively with both terminal oxygens, which from our computational point of view is equivalent to having two open reactive channels, although the products are indistinguishable. In fact, there is another possible reaction channel that gives rise to the products HO_2 + O, but up to a translational energy of 0.4 eV its occurrence is considered to be negligible.[20] To account for all such possibilities, three negative imaginary terms (of the linear Baer−Neuhauser ramp potential type[47]) are added to the real Hamiltonian: two vibrational terms iv_{Ir} and $iv_{I\rho}$ and a translational term iv_{IR}, namely

$$V_I(r,\rho,R) \equiv -i[v_{Ir}(r) + v_{I\rho}(\rho) + v_{IR}(R)] \quad (17)$$

The full-dimensional solution of eq 5 requires nevertheless a large computational effort even for much simpler systems like HHOH.[52,53] As shown in ref 52 for the former case, the IOSA method proposed here may be more efficient than other methods because freezing the angular coordinates saves us from treating explicitly the angular operators, thus reducing significantly both the programming efforts and the consumption of computer time. In addition, due to the potential energy surface polar-averaging, we can avoid randomizing the angle β as required by the standard IOSA method and hence reduce further the computational labor.

Returning to the derivation of the inhomogeneity function χ_{t_0}, the addition of the NIPs to the real averaged potential $\bar{U}$ converts the scattering problem into a bound system problem and hence makes χ_{t_0} expandable in terms of square integrable L^2 functions.[54,55] These functions are chosen here as localized functions for the translational components and adiabatic basis sets for the vibrational ones. Thus,

$$\chi^J_{t_0}(r\rho R\theta\gamma|jK) = \frac{1}{r\rho R}\sum_{nt} a^J_{nt} g(R|n)\, f(r\rho\theta\gamma|jK|nt) \quad (18)$$

where $g(R|n)$ represents the translational component which is chosen to be a standard Gaussian function of the form

$$g(R|n) = \left(\frac{\alpha}{\sigma\sqrt{\pi}}\right)^{1/2} \exp\left[-\frac{\alpha^2}{2}\left(\frac{R-R_n}{\sigma}\right)^2\right] \quad (19)$$

where σ is the translational step size,

$$\sigma = R_n - R_{n-1} \quad (20)$$

Regarding $f(r\rho\theta\gamma|jK|nt)$, it is an eigenfunction of the 3D Schrödinger equation

$$\left[-\frac{\hbar^2}{2mr}\frac{\partial^2}{\partial r^2}r - \frac{\hbar^2}{2\mu\rho}\frac{\partial^2}{\partial \rho^2}\rho + \hbar^2\left(\frac{1}{2mr^2} + \frac{1}{2\mu\rho^2}\right)j(j+1) + \frac{\hbar^2}{2\mu\rho^2}K(K+1) + \bar{U}(r\rho R_n\theta\gamma) - \epsilon(t|\theta\gamma jK|R_n)\right] f(r\rho\theta\gamma|jK|nt) = 0 \quad (21)$$

Once eq 21 has been solved, it is then possible, starting from eq 3, to obtain the γ -dependent $\boldsymbol{S}$ matrix element. Finally, to obtain the reactive probabilities, the following average is required:

$$\langle|S^J(t\leftarrow t_0)|^2\rangle = \frac{1}{2}\int_{-1}^{1}|S^J(t\leftarrow t_0)|_\gamma|^2 \, d\cos\gamma \quad (22)$$

4. Numerical Details

In this work, we have carried out quantum dynamical computations of nonreactive probabilities for the H + O_3 process over the range of translational energies 0.05−0.35 eV using the DMBE HO_3 potential energy surface of Varandas and Yu.[20] The consecutive reactive probabilities have then been computed

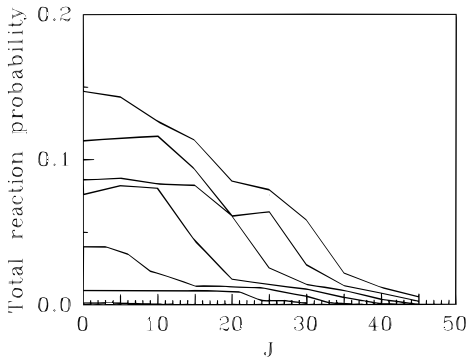

Figure 3. Opacity functions calculated as a function of the total angular momentum. Curves have been computed for values of E_{tr} ranging from 0.05 to 0.35 eV at steps of 0.05 eV, which can be identified in ascending order by going from bottom to top at $J = 0$.

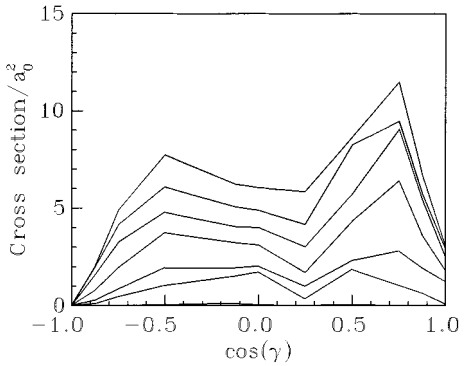

Figure 4. Angular distribution of total cross sections as a function of the angle γ (see Figure 2). Curves are shown for the same translational energies as in Figure 3 and can be identified for increasing values of E_{tr} by going from bottom to top at $\cos(\gamma) \approx -0.25$.

by means of eq 1 and wholly attributed to the reaction leading to $HO + O_2$ products.

The calculations have generally been carried out within the j_z approximation using a polar-averaged expression of the potential energy surface. However, to derive χ_{t_0} (the perturbed part of the total wave function in the reagents' arrangement channel), the parameter γ (the angle between the translational coordinate R and the ozone "translational" coordinate ρ) has been treated as an IOSA parameter. The probabilities thus obtained have then been numerically averaged as indicated in eq 22 by dividing the integration region of cos γ into 10 equidistant grids.

To solve eq 5 (for a given ψ_{t_0}), the R translational axis has been divided into 50 equidistant sectors. In each of them one Gaussian, standing as a translational basis function, and a set of 2-fold adiabatic vibrational basis functions are used (see eq 18). The number of such functions varies from one sector to another, but at each sector their number is constrained by a simple energy value of 10 eV.[48,55] This implies solving about 5000 complex equations in order to obtain the coefficients mentioned.

5. Results

Figure 3 shows the calculated reactivion probabilities for the title reaction as a function of the total angular momentum. The results are presented for values of E_{tr} which range from 0.05 to 0.35 eV at intervals of 0.05 eV. In all cases the calculated opacity function shows a maximum at $J = 0$ and decreases to zero at a cutoff J value which increases with increasing energy.

In Figure 4 are presented the γ -dependent cross sections. It is seen that the reaction is most favorable for $\gamma = 30°$ and 120°,

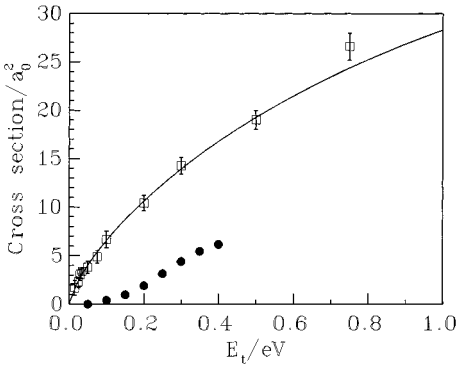

Figure 5. Cross section as a function of translational energy for the process $H + O_3 \rightarrow HO + O_2$. A comparison between QM and QCT is shown. The full line indicates the fit to the actual QCT results, which are indicated by the open squares; also shown are the corresponding error bars. The QM results are indicated by the solid dots.

which correspond[20] approximately to the most favorable orientations for H to attack one of the terminal atoms of ozone. Conversely, the reactivity is seen to attain a minimum value for $\gamma \simeq 0°$ and 180°, which correspond to nearly linear $H-O_a-O_b$ and $H-O_c-O_b$ arrangements; the indices *a*, *b*, and *c* label the oxygen atoms, with *b* denoting the middle atom in O_3.

The calculated cross sections for the $H + O_3 \rightarrow HO + O_2$ reaction as a function of translational energy are shown in Figure 5. Also shown are the QCT results[20,21] using the same HO_3 DMBE potential energy surface. As seen, the QCT results clearly overestimate the quantum dynamical ones, particularly near threshold. This general trend has also been observed for atom+triatom reactions on other occasions[23,52] (for atom+diatom reactions, see, for example, ref 56 and references therein), and it is partly attributed to zero-point energy leakage. While the zero-point vibrational energy is kept constant in quantum dynamics, it becomes available to promote reaction in QCT calculations. Such a feature is therefore expected to be particularly effective at the threshold region. Other reasons for the discrepancy can be due to the fact that the quantum mechanical treatment is done with reduced dimensionality.

Figure 5 shows the calculated thermal rate coefficients as a function of temperature over the range $100 \leq T/K \leq 700$. Also included for comparison are the available experimental estimates and the results of QCT calculations[20] based on the same HO_3 DMBE potential energy surface. Regarding the agreement with the experimental data, the general trend is satisfactory, with the experimental data falling in between the classical and quantum mechanical results. Note that the agreement of the latter is best with the data of Clyne and Monkhouse,[5] which cover the range of temperatures $300 \leq T/K \leq 650$, and the recent measurement of Greenblatt and Wiesenfeld[8] for $T = 300$ K. However, it is a factor of 5 or so too small when compared with the recommended value[57] for $T = 300$ K. The activation energy predicted from the present work ($\sim$0.63 kcal mol^{-1}) is also found to be in satisfactory agreement with the estimate from the experimental data[57] (0.9−1.5 kcal mol^{-1}) and the QCT value[20,21] (0.75 kcal mol^{-1}). A final comment is made for the classical versus quantum comparison. As seen from Figure 6, the quantum rate constants underestimate the classical ones by a factor of 5 or so over the entire range of temperatures. This may be rationalized from the behavior of the excitation function at low energies since these dominate the calculation of the thermal rate coefficient for the temperatures considered in the present work.

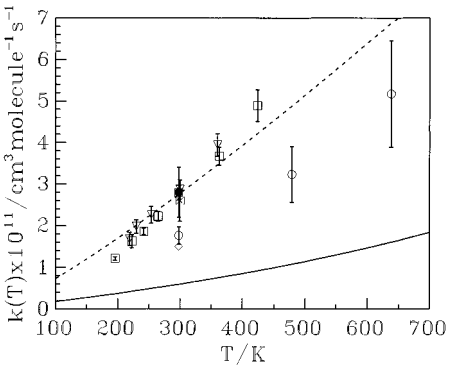

Figure 6. Linear plot of the rate constant as a function of *T*: full line, QM results; dashed line, QCT results. Experimental results: open diamond, ref 8; open circles, ref 5; down triangles, ref 7; bowtie, ref 6, open squares, ref 4. Shown by the solid dot is the recommended value of ref 57.

6. Conclusions

We have carried out three-dimensional quantum dynamics calculations of the reaction H + O_3 → HO + O_2 using a recently reported[20] DMBE potential energy surface for the ground electronic state of HO_3. The calculated rate coefficient and activation energy have been found to be in reasonable agreement with the experimental results, especially with the data of Clyne and Monkhouse[5] and Greenblatt and Wiesenfeld.[8] The present quantum dynamics calculations have also been compared with the results of QCT calculations based on the same HO_3 DMBE potential energy surface. The agreement observed between the quantum and classical results is also moderate, with the largest discrepancies occurring near threshold. Such discrepancies have been tentatively attributed both to the approximations involved in the quantum approach of the present work and to zero-point energy leakage near threshold in classical dynamics. Needless to say, some of the discrepancies between theory and experiment can also be due to inaccuracies of the potential energy surface. Unfortunately, the scatter of the experimental results is sufficiently large to invalidate a definite conclusion about which theory performs best for the title reaction or to suggest defficiencies of the potential energy surface. Thus, it also prevents any serious attempt to improve the potential energy surface from the rate constant results. Of course, the scatter of experimental data does not invalidate the quantum versus classical comparison reported in the present work since both calculations have employed the same potential energy surface.

Acknowledgment. This work has been supported by the Junta Nacional de Investigação Científica e Tecnológica, Portugal, under program PRAXIS XXI (Contract 2/2.1/QUI/408/94). It has also benefited from an EC grant, under Contract CHRX-CT 94-0436.

References and Notes

(1) Charters, P. E.; Macdonald, R. G.; Polanyi, J. C. *Appl. Opt.* **1971**, *10*, 1747.
(2) Anlauf, K. G.; Macdonald, R. G.; Polanyi, J. C. *Chem. Phys. Lett.* **1968**, *1*, 619.
(3) Polanyi, J. C.; Sloan, J. J. *Int. J. Chem. Kinet. Symp.* **1975**, *1*, 51.
(4) Keyser, L. F. *J. Phys. Chem.* **1979**, *83*, 645.
(5) Clyne, M. A. A.; Monkhouse, P. B. *J. Chem. Soc., Faraday Trans. 2* **1977**, *73*, 298.
(6) Phillips, L. F.; Schiff, H. I. *J. Chem. Phys.* **1962**, *37*, 1233.
(7) Lee, J. H.; Michael, J. V.; Payne, W. A.; Stief, L. J. *J. Chem. Phys.* **1978**, *69*, 350.
(8) Greenblatt, G. D.; Wiesenfeld, J. R. *J. Geophys. Res.* **1982**, *87*, 11145.
(9) Finlayson-Pitts, B. J.; Kleindienst, T. E.; Ezell, M. J.; Toohey, D. W. *J. Chem. Phys.* **1981**, *74*, 4533.
(10) Washida, N.; Akimoto, H.; Okuda, M. *J. Chem. Phys.* **1980**, *72*, 5781.
(11) Finlayson-Pitts, B. J.; Kleindienst, T. E. *J. Chem. Phys.* **1979**, *70*, 4804.
(12) Howard, C. J.; Finlayson, B. J. *J. Chem. Phys.* **1980**, *72*, 3842.
(13) Force, A. P.; Wiesenfeld, J. R. *J. Chem. Phys.* **1981**, *74*, 1718.
(14) Bates, D. R.; Nicolet, M. *J. Geophys. Res.* **1950**, *55*, 301.
(15) Herzberg, G. *J. R. Astron. Soc. Can.* **1951**, *45*, 100.
(16) Meinel, A. B. *Astrophys. J.* **1950**, *111*, 555.
(17) Meinel, A. B. *Astrophys. J.* **1950**, *112*, 120.
(18) Ohoyama, H.; Kasai, T.; Yoshimura, Y.; Kuwata, H. *Chem. Phys. Lett.* **1985**, *118*, 263.
(19) Klenerman, D.; Smith, I. W. M. *J. Chem. Soc., Faraday Trans. 2* **1987**, *83*, 229.
(20) Varandas, A. J. C.; Yu, H. G. *Mol. Phys.* **1997**, *91*, 301.
(21) Yu, H. G.; Varandas, A. J. C. *J. Chem. Soc., Faraday Trans.* **1997**, *93*, 2651.
(22) Varandas, A. J. C. *Adv. Chem. Phys.* **1988**, *74*, 255.
(23) Szichman, H.; Baer, M. *J. Chem. Phys.* **1996**, *105*, 10380.
(24) Szichman, H.; Varandas, A. J. C.; Baer, M. *Chem. Phys. Lett.* **1994**, *231*, 253.
(25) Szichman, H.; Varandas, A. J. C.; Baer, M. *J. Chem. Phys.* **1995**, *102*, 3474.
(26) Szichman, H.; Baer, M. *Chem. Phys. Lett.* **1995**, *242*, 285.
(27) Takayanagi, T. *Bull. Chem. Soc. Jpn.* **1995**, *68*, 2527.
(28) Schatz, G. C. *Chem. Rev.* **1987**, *87*, 81.
(29) Bowman, J. M.; Gazdy, B.; Sun, Q. *J. Chem. Phys.* **1989**, *91*, 2859.
(30) Miller, W. H.; Hase, W. L.; Darling, C. L. *J. Chem. Phys.* **1989**, *91*, 2863.
(31) Nyman, G.; Davidsson, J. *J. Chem. Phys.* **1990**, *92*, 2415.
(32) Alimi, R.; García-Vela, A.; Gerber, R. B. *J. Chem. Phys.* **1992**, *96*, 2034.
(33) Varandas, A. J. C.; Marques, J. M. C. *J. Chem. Phys.* **1992**, *97*, 4050.
(34) Varandas, A. J. C. *J. Chem. Phys.* **1993**, *99*, 1076.
(35) Peslherbe, G. H.; Hase, W. L. *J. Chem. Phys.* **1994**, *100*, 1179.
(36) Varandas, A. J. C.; Marques, J. M. C. *J. Chem. Phys.* **1994**, *100*, 1908.
(37) Varandas, A. J. C. *Chem. Phys. Lett.* **1994**, *225*, 18.
(38) Ben-Num, M.; Levine, R. D. *J. Chem. Phys.* **1994**, *101*, 8768.
(39) Lim, K. F.; McCormack, D. A. *J. Chem. Phys.* **1995**, *102*, 1705.
(40) Kumar, S.; Sathyamurthy, N.; Ramaswamy, R. *J. Chem. Phys.* **1995**, *103*, 6021.
(41) Schlier, C. *J. Chem. Phys.* **1995**, *103*, 1989.
(42) McCormack, D. A.; Lim, K. F. *J. Chem. Phys.* **1995**, *103*, 1991.
(43) Guo, Y.; Thompson, D. L.; Sewell, T. D. *J. Chem. Phys.* **1996**, *104*, 576.
(44) Ben-Nun, M.; Levine, R. D. *J. Chem. Phys.* **1996**, *105*, 8136.
(45) McCormack, D. A.; Lim, K. F. *J. Chem. Phys.* **1997**, *106*, 572.
(46) Lim, K. F. *J. Chem. Soc., Faraday Trans.* **1997**, *93*, 669.
(47) Neuhauser, D.; Baer, M. *J. Chem. Phys.* **1989**, *90*, 4351.
(48) Szichman, H.; Baer, M. *J. Chem. Phys.* **1994**, *101*, 2081.
(49) Murrell, J. N.; Sorbie, K. S.; Varandas, A. J. C. *Mol. Phys.* **1976**, *32*, 1359.
(50) McGuire, P.; Kouri, D. J. *J. Chem. Phys.* **1974**, *60*, 2488.
(51) Pack, R.T *J. Chem. Phys.* **1974**, *60*, 633.
(52) Zhang, D. H.; Light, J. C. *J. Chem. Phys.* **1996**, *104*, 4544.
(53) Zhang, D. H.; Light, J. C. *J. Chem. Phys.* **1996**, *105*, 1291.
(54) Szichman, H.; Last, I.; Baram, A.; Baer, M. *J. Phys. Chem.* **1993**, *97*, 6436.
(55) Last, I.; Baram, A.; Szichman, H.; Baer, M. *J. Phys. Chem.* **1993**, *97*, 7040.
(56) Varandas, A. J. C. *Chem. Phys. Lett.* **1995**, *235*, 111.
(57) Baulch, D. L.; Cox, R. A.; Crutzen, P. J.; Hampson, R. F., Jr.; Kerr, J. A.; Troe, J.; Watson, R. T. *J. Phys. Chem. Ref. Data* **1982**, *11*, 327.